CORA Cork Open Research Archive
Cartlann Taighde Oscailte Chorcaí

Title	Modification of emission of CdTe nanocrystals by the local field of Langmuir-Blodgett colloidal photonic crystals
Authors	Romanov, Sergei G.;Bardosova, Maria;Povey, Ian M.;Torres, C. M. Sotomayor;Pemble, Martyn E.;Gaponik, Nikolai;Eychmueller, Alexander
Publication date	2008-11-26
Original Citation	Romanov, S. G., Bardosova, M., Povey, I. M., Torres, C. M. S., Pemble, M. E., Gaponik, N. and Eychmüller, A. (2008) 'Modification of emission of CdTe nanocrystals by the local field of Langmuir–Blodgett colloidal photonic crystals', Journal of Applied Physics, 104(10), pp. 103118. doi: 10.1063/1.2981087
Type of publication	Article (peer-reviewed)
Link to publisher's version	http://aip.scitation.org/doi/abs/10.1063/1.2981087 - 10.1063/1.2981087
Rights	© 2008 American Institute of Physics, This article may be downloaded for personal use only. Any other use requires prior permission of the author and AIP Publishing. The following article appeared in Romanov, S. G., Bardosova, M., Povey, I. M., Torres, C. M. S., Pemble, M. E., Gaponik, N. and Eychmüller, A. (2008) 'Modification of emission of CdTe nanocrystals by the local field of Langmuir–Blodgett colloidal photonic crystals', Journal of Applied Physics, 104(10), pp. 103118 and may be found at http://aip.scitation.org/doi/abs/10.1063/1.2981087
Download date	2024-04-20 15:23:05
Item downloaded from	https://hdl.handle.net/10468/4220

UCC

University College Cork, Ireland

Coláiste na hOllscoile Corcaigh

Modification of emission of CdTe nanocrystals by the local field of Langmuir–Blodgett colloidal photonic crystals

Sergei G. Romanov' , Maria Bardosova, Ian M. Povey, C. M. Sotomayor Torres, Martyn E. Pemble, Nikolai Gaponik, and Alexander Eychmüller

Citation: Journal of Applied Physics **104**, 103118 (2008); doi: 10.1063/1.2981087
View online: http://dx.doi.org/10.1063/1.2981087
View Table of Contents: http://aip.scitation.org/toc/jap/104/10
Published by the American Institute of Physics

Modification of emission of CdTe nanocrystals by the local field of Langmuir–Blodgett colloidal photonic crystals

Sergei G. Romanov,[1,a)] Maria Bardosova,[2] Ian M. Povey,[2] C. M. Sotomayor Torres,[2] Martyn E. Pemble,[2] Nikolai Gaponik,[3] and Alexander Eychmüller[3]
[1]*Ioffe Physical Technical Institute, Polytekhnicheskaya st., 26 194021, St. Petersburg, Russia*
[2]*Tyndall National Institute, University College Cork, Prospect Row, Cork, Ireland*
[3]*Institute of Physical Chemistry and Electrochemistry, Technical University of Dresden, Bergstr. 66b, Dresden 01062, Germany*

(Received 16 April 2008; accepted 23 July 2008; published online 26 November 2008)

A light source on the surface of a slab of 2+1-dimensional photonic crystal has been prepared by the Langmuir–Blodgett deposition of a colloidal crystal on top of a thin film containing CdTe nanocrystals. The directional enhancement of the light emission intensity in the spectral range of the photonic bandgap has been revealed through the comparative examination of the angle-resolved transmission, diffraction, and photoluminescence spectra of the prepared structures. Changes in the emission spectrum have been tentatively explained in terms of the acceleration of the radiative recombination due to the increase in the local field strength at photonic bandgap resonance and changes in the emission diagram—as arising from the wavelength dependence of the topology of the local field pattern. © *2008 American Institute of Physics*. [DOI: 10.1063/1.2981087]

I. INTRODUCTION

The control over the emission spectrum and directionality of light sources can be achieved by tailoring their electromagnetic environment, for example, with the help of photonic crystals (PhCs).[1] If a light source is embedded in a finite size three-dimensional (3D) PhC, its spontaneous emission becomes suppressed in the spectral range of a directional photonic bandgap (PBG) due to the reduction in the number of optical modes, by which the emission can be transported.[2] In this case, the angle-resolved spectrum of emission intensity follows the PBG-related transmission minimum (Fig. 1). Since the PBG corresponds to the minimum in the density of photon modes, the mode density peaks at the edges of a PBG or at a defect mode inside the PBG. Such peaks facilitate the increase in the emission rate.[3,4]

If a light source is spatially separated from a PhC, their interaction essentially remains but it rapidly decreases with increasing PhC to source distance.[5] The emission rate enhancement is expected to be in the same PBG frequency range due to an increase in the evanescent field strength at the PhC surface. In this case, the correlation between the transmission and emission spectra may be opposite to the case of a PhC-embedded source (Fig. 1). In particular, the dipole transition probability of an oscillator placed in between a two-dimensional (2D) colloidal crystal and a dielectric substrate depends on the emitter position with respect to the local field pattern; hence, the emission of a light source radiated in the near-field zone at the PhC boundary can be either enhanced or suppressed.[6,7] Visualization of such local field patterns at the surface of colloidal crystals has been made using the near-field optical microscopy.[8,9]

The PBG emission enhancement should not be confused with traditional ways of increasing the brightness of light emitting devices based on exploiting grating couplers and randomly textured surfaces.[10,11] The latter approach addresses the external quantum efficiency by extracting that fraction of the emission, which is trapped in the structure due to the total internal reflectance. With the increase in the refractive index (RI) contrast, such gratings can be considered in terms of 2D PhCs, in which the wave optics phenomena coexist with geometrical optics.[12] To date, the efficient outcoupling of radiation has been realized by coupling the radiation to leaky guided modes with frequencies above the light cone in emitters nanopatterned as 2D PhCs.[13]

From a technology point of view, the sandwiched emitter-PhC structures look simpler compared to emitter-impregnated PhCs, but their design and operation need detailed investigation. First, the light source should be thin enough to be contained in the near-field zone of the PhC. Promising light sources have been recently developed using colloidal semiconductor nanocrystals (NCs). In particular, NCs were used for impregnation of direct[14] and inverted

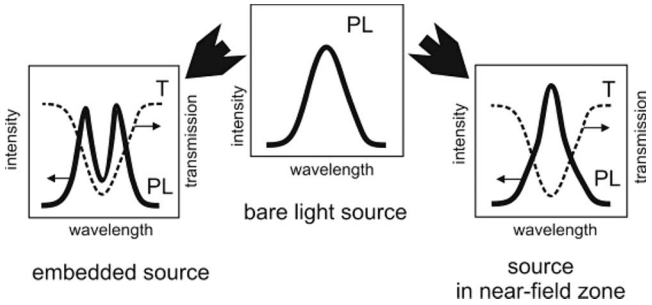

FIG. 1. Schematics of the spontaneous emission spectrum modification for the light source inside a 3D PhC (left) and at the surface of 3D PhC (right). The dotted lines show the transmission spectra with the PBG minimum on a stack of PhC planes (left) and with the minimum due to excitation of surface modes (right).

[a)]Author to whom correspondence should be addressed. Electronic mail: sergei.romanov@tyndall.ie.

 © 2008 American Institute of Physics

opal-based PhCs.[15,16] In this work we used NCs encapsulated in layer-by-layer (LbL) deposited polyelectrolyte films.[17] The thickness of such sources remains within a few tens of nanometers. These NC-based emitters possess the RI of the same 1.6–1.9 magnitude as is typical for organic light emitting devices,[18] but offer a narrower and easily adjustable emission band. Second, the chosen PhC should have a tunable PBG over a broad spectral range, the PhC formation should be controllable, and the preparation method should be compatible with a broad variety of light sources. Colloidal PhCs satisfy these conditions, their PBG is adjustable over the visible and near infrared, and their technology allows one to avoid the cost and complexity of nanolithography.[19] Colloidal PhCs can be directly deposited on the surface of the light emitting film using the well-controllable Langmuir–Blodgett (LB) technique.[20] When compared to micromanipulation[21] or colloidal self-assembly,[19] the LB method offers large area coatings and precision in terms of depositing the required number of monolayers of spheres.

In this paper, we report the effect of LB colloidal crystal films on the spontaneous emission of CdTe NC-based light sources. The structure of this paper is as follows: In Sec. II we describe the sample preparation and the measurement technique; in Sec. III the spectral changes of the emission from a PhC-coupled light source are considered; and in Sec. IV we demonstrate changes in the emission directionality. The discussion in Sec. V provides arguments in favor of the local field mechanism of the observed emission modifications.

II. EXPERIMENTAL TECHNIQUE

Uniform thin films containing size-selected 2 nm CdTe NCs (Ref. 22) were prepared by LbL assembly.[17] The following cyclic procedure was used: (i) dipping of the glass substrate into a solution (5 mg/ml in 0.2 M NaCl) of poly-(diallyldimethylammonium) chloride for 10 min; (ii) rinsing with water for 1 min; (iii) dipping into aqueous dispersions of the negatively charged NCs (ca. 10^{-6} M) for 10 min; and (iv) rinsing with water again for 1 min. Each cycle of this procedure results in a "bilayer" consisting of a polymer/NC composite. Twenty bilayers were deposited in order to increase the brightness of luminescence. The thickness of a 20 bilayer film is about 60 nm. Since the volume fraction of NCs is about 27%, the average RI of the polyelectrolyte-CdTe film is about 1.9. What follows these films will be referred to as NC films (NCFs).

Silica spheres of the nominal diameter $D=519$ nm were fabricated using the Stöber technique.[23] These spheres were hydrophobized with 3-trimethoxysilylpropyl methacrylate. The LB technique with a low barrier speed of 6 $cm^2\ min^{-1}$ was used to compress sphere arrays in hexagonally packed monolayers (1L) on the surface of doubly distilled deionized water and to transfer them to the substrate. Using this technique, the monolayer of spheres was deposited at a surface pressure of 4 mN/m (Ref. 24) onto the LbL NCF substrate (see the inset of Fig. 2). Subsequent monolayers were deposited after drying the deposited ones. Both mono- and multiple layers [up to five layers (5L)] of the SiO_2 spheres

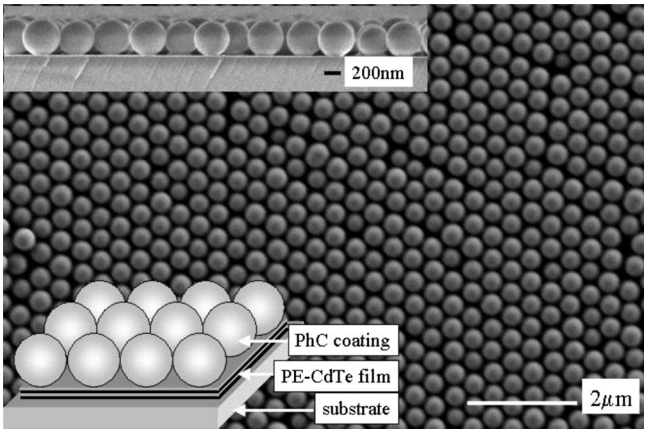

FIG. 2. SEM image of a LB monolayer of 519 nm silica spheres on a glass substrate. Insets: top—side view of LB monolayer and bottom—schematics of the studied structures consisting of a glass substrate with LbL deposited CdTe NCF and LB deposited monolayer of silica spheres.

were prepared. Monolayers of spheres form the LB colloidal PhC possessing the PBG of (2+1) dimensionality. Although no 3D lattice is formed due to lack of lateral alignment between monolayers, the LB crystal remains ordered within each monolayer of spheres and as a periodic stack of monolayers (Fig. 2).[25,26]

Angle-resolved transmission spectra were acquired by illuminating the structures with a collimated 1 mm in diameter beam of a white light from a tungsten lamp at different angles, θ, of incidence with respect to the film normal. Transmitted light was collected from a cone of about 2° of angular width. Transmission spectra were obtained at angles of θ between 0° and 60° for the orthogonal *s*- and *p*-polarizations.

The surface diffraction spectra were obtained by directing a beam of white light at a certain angle of incidence and collecting spectra at different angles α, keeping constant the sum of the angles of incidence, θ, and diffraction, α. Both angles were measured with respect to the normal to the LB crystal plane.

The photoluminescence (PL) spectra of NCFs were generated by excitation by the 457.9 nm line of an Ar-ion laser. A laser spot size of 5 mm in diameter was selected in order to mimic the emission from a large-area display. The excitation conditions, the laser power and the spot size, were maintained constant at all angles of the emission detection in order to eliminate excitation-related variation in the PL spectra. The light collection cone was restricted to 6° by an aperture between the sample and the collecting lens. Emission was collected in the forward direction by exciting the NCF through the substrate and detecting after passing the PhC film and in the backward direction—by detecting the emission, which does not traverse the PhC film.

III. TRANSMISSION VERSUS EMISSION SPECTRA OF SANDWICH STRUCTURES

The *s*-polarized far-field transmission spectrum of an LB packed monolayer of spheres on a glass substrate [Fig. 3(a)] shows the well-defined minimum of 0.08 relative bandwidth centered at 548 nm, which provides 12% attenuation of the light incident on a film along the film normal. The central

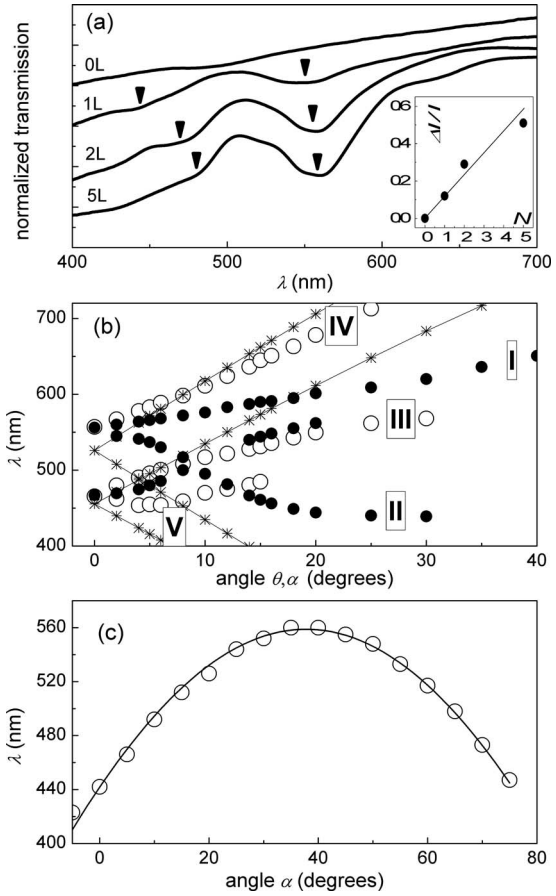

FIG. 3. (a) Transmission spectra of samples with different numbers, N, of sphere monolayers along the LB coating normal. Inset—relative light attenuation at the transmission minimum as a function of N. (b) Angular dispersion of transmission minima of 2L LB PhC in s- (solid circles) and p- (open circles) polarized lights. Numbers indicate dispersion branches. Stars show the dispersions obtained according to formula (1) along two principal directions in the trigonal lattice of spheres. (c) Angular dispersion of surface diffraction maxima (circles) and its approximation by expression (1) (line).

wavelength of this minimum increases slightly with the increasing number of layers N. For multiple-layer coatings, the transmission significantly decreases toward shorter wavelengths due to light scattering at package irregularities. Transmission spectra of samples with multilayer coatings demonstrate the increase in the relative attenuation $\Delta I/I_0$ in the minimum with increasing N as $\Delta I/I_0 \sim N^{0.9}$ [see the inset of Fig. 3(a)], where I_0 is the extrapolated transmission in the absence of the minimum. This, practically, linear dependence shows that the attenuation is an additive function per number of layers. Additional shallow minima were detected at approximately 444, 470, and 481 nm for the 1L, 2L, and 5L coatings, respectively [Fig. 3(a)]. The 2L and 5L coatings also possess the transmission minimum centered at 1093 nm due to the Bragg diffraction on a stack of sphere monolayers,[25] which is not shown in Fig. 3.

Figure 3(b) shows the angular dispersion of the transmission minima in a 2L LB-coated sample. There are several branches; moreover, the I, II, and IV branches, as well as the III and V branches, are degenerate at $\theta=0°$. The dispersion of the surface diffraction resonance observed in this sample is shown in Fig. 3(c).

The emission band of the NCF assembled from 2 nm in

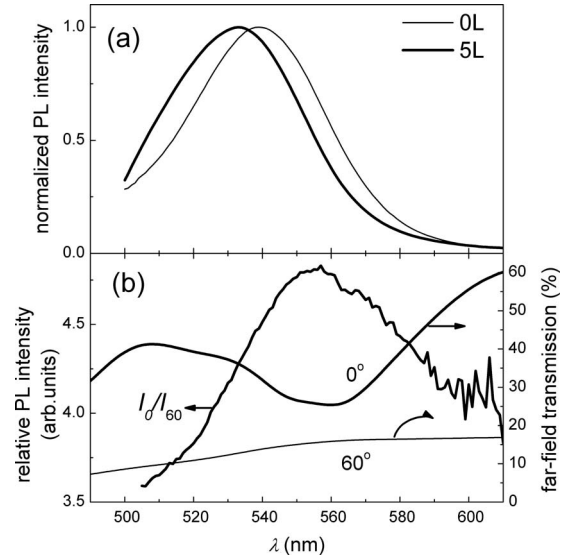

FIG. 4. (a) Normalized PL spectra of bare NCF (thin line) and 5L LB-coated NCF (thick line) at $\theta=0°$ angle of emission detection. (b) Relative PL spectrum in comparison to far-field transmission spectra obtained at angles $\theta=0°$ and 60°.

diameter CdTe NCs is centered at 540 nm [Fig. 4(a)]. The relative full width at half maximum (FWHM) is 0.85. At $\theta=0°$ the emission band of the 5L-coated NCF is centered at 533 nm with a 0.09 FWHM. The blueshift of the emission band of the LB-coated NCF, with respect to that of the bare NCF, is the result of the PhC coating. This was proved by the multiplication of the PL spectrum of the bare NCF by the transmission spectrum of the 5L PhC reproducing such a band shift. The broadening of the PL band of LB-coated NCF could be induced by the chemical modification of the CdTe NC surface during the course of the LB film deposition. PL spectra of the LB-coated NCFs look similar for the different numbers of LB monolayers. The relative PL spectrum obtained as the ratio of PL spectra, $I(\lambda)_{\theta=0}/I(\lambda)_{\theta=60}$, shows the maximum centered at 555 nm, which coincides with the minimum in the transmission spectrum [Fig. 4(b)]. The angle-resolved PL spectrum at $\theta=60°$ was used as the reference because the corresponding far-field angle-resolved transmission spectrum is flat in this wavelength range [Fig. 4(b)].

This correlation between far-field transmission and PL spectra remains valid for detection angles $0° \leq \theta \leq 20°$ [Figs. 5(a) and 5(b)]. It is worth noting that the PhC-induced modulation of the PL intensity is proportional to the attenuation in the transmission minimum, i.e., increasing the observation angle decreases the attenuation leading to a vanishing PL spectrum modulation [Fig. 5(b)]. In the case of the uncoated NCF no angular dependence of the PL spectrum was detected [Fig. 5(c)].

IV. ANGLE DIAGRAMS OF THE EMISSION INTENSITY

The PL intensity at a given wavelength plotted as a function of the angle of detection, $I_\lambda(\theta)$, represents the emission indicatrix. The $I_\lambda(\theta)$ plots of a 2L-coated NCF obtained at wavelengths of 510, 550, and 590 nm are shown in Fig. 6, together with their corresponding far-field transmission dia-

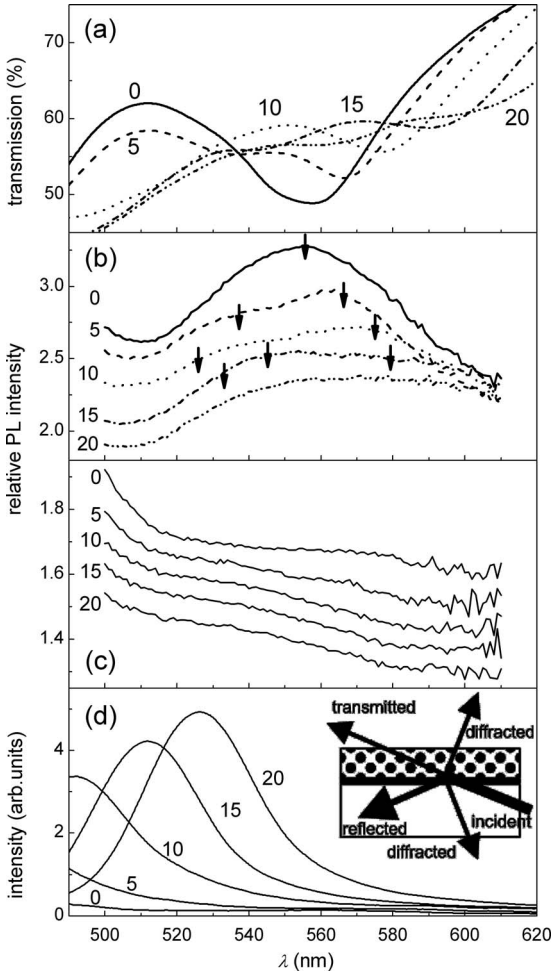

FIG. 5. (a) Angle-resolved transmission spectra of *s*-polarized light. Numbers show the angles of light incidence. (b) Angle-resolved relative PL spectra of 2L LB-coated NCF in the forward direction through the LB crystal (thick lines). Numbers correspond to the angle of detection. Arrows indicate the centers of transmission minima according to Fig. 3(b). (c) Angle-resolved PL spectra of the uncoated NCF. Numbers correspond to the angle of detection. (d) Diffraction spectra at angles α shown at curves. Inset: schematic of the light transmission and the first order diffraction in LB coating.

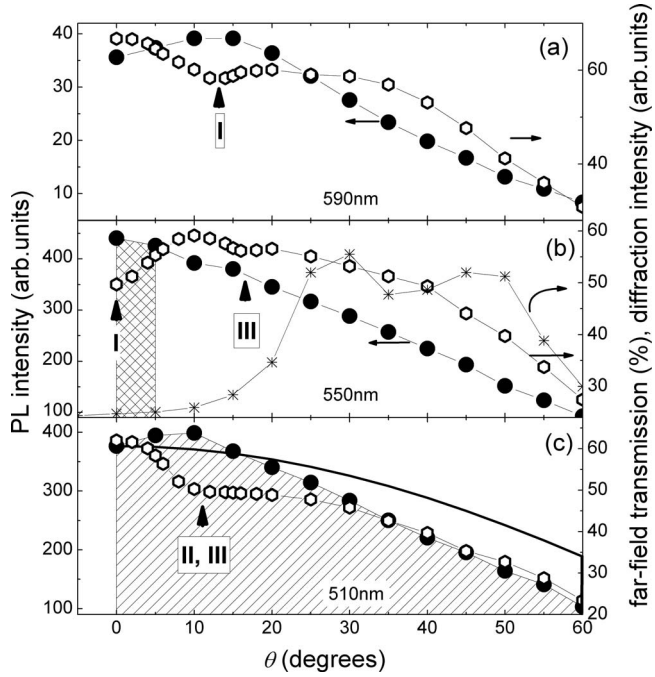

FIG. 6. Angle diagrams of emission intensity (solid circles) at $\lambda=590$, 550, and 510 nm in comparison to diagrams of transmission at the same wavelengths (open hexagons). These diagrams are compared to the angle diagram of diffraction intensity at $\lambda=550$ nm (stars) in panel (b) and the Lambert diagram (line) in panel (c). Shaded areas show the emission power between (b) 0° and 5°—S^5_{550} and (c) 0° and 60°—S^{60}_{510}. Arrows mark the angle position of transmission minima. Numbers at arrows indicate the dispersion branch as indicated in Fig. 3(b).

grams $T_\lambda(\theta)$. The transmission directionality diagrams show the transmission minima [Fig. 3(b)] superimposed on a smooth background. The angular width of the transmission minimum is less than $\pm 10°$ with respect to the midgap direction. The comparison of emission and transmission diagrams reveals that the PL intensity peaks along the direction of the far-field transmission minimum. This observation correlates with the observation of the relative PL maximum at wavelengths of the far-field transmission minimum (Fig. 4). It is worth noting that the $I_\lambda(\theta)$ in the studied samples does not follow the Lambert diagram $I_\lambda \propto \cos\theta$ [Fig. 6(c)].

To quantify the radiation power emitted by the NCF, we calculated the total area under the angle diagram $S^{60}_\lambda = \int_{\Delta\lambda} I_\lambda(\theta)d\theta$, where the angle interval, $\Delta\theta$, is from 0° to 60° [Fig. 6(c)]. Assuming the even azimuth distribution of the emission intensity and taking into account that the emission intensity becomes sufficiently low at $\theta \geq 60°$, the S^{60}_λ is proportional to the power radiated at a given wavelength. The integration of the S^{60}_λ over the studied spectral range is proportional to the total emitted flux.

In order to characterize the overall effect of PhC coating upon the emission directionality, we normalized the S^{60}_λ area to that under the Lambert-type diagram, $S^L_\lambda = \int_{\Delta\theta} I(\lambda, \theta=0°)\cos\theta d\theta$, where the intensity $I(\lambda, \theta=0°)$ is taken from the experimental data and $\Delta\theta=60°$. The spectrum of the ratio $S^{60}_\lambda / S^L_\lambda$ shows that the spectral range, where the LB coating changes the NCF emission, is the PBG spectral range of the LB PhC. This is because the spectrum $S^{60}_\lambda / S^L_\lambda$ of the 2L-coated NCF follows the far-field transmission spectrum obtained along the film normal (Fig. 7). In contrast, the emission directionality of the bare NCF diagram is gradually squeezed with increasing wavelength. The width of the PL indicatrix of the LB-coated NCF is reduced by 14% at PBG wavelengths compared to that at wavelengths outside the PBG. Similar observations apply to samples with the 1L and 5L coatings.

In order to map the emission extraction in the angle-wavelength plane, we calculated the quantity, S^5_λ, which is proportional to the emission flux propagating within the angular cone $\Delta\theta$ from 0° to 5° at a given wavelength along the film normal. S^5_λ was then normalized to S^{60}_λ to obtain the extraction fraction $S^5_\lambda / S^{60}_\lambda$. The spectrum of $S^5_\lambda / S^{60}_\lambda$ shows that the spectral band, where the extraction is enhanced along the film normal, is centered at 555 nm in coincidence with the central wavelength of the far-field transmission minimum (Fig. 8). Similar extraction bands were observed

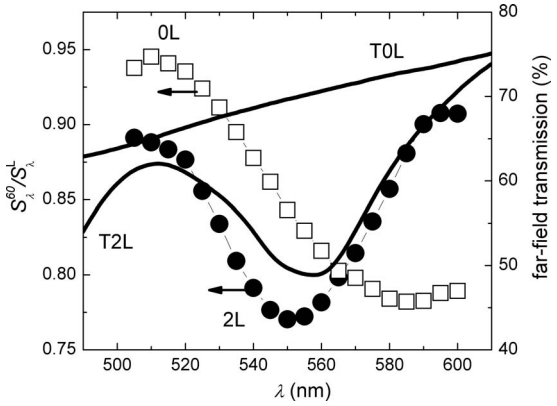

FIG. 7. The spectrum of the relative directionality of the emission flux with respect to that of the Lambert-type flux directionality in the case of the bare (squares) and the 2L LB-coated (circles) NCFs. Far-field transmission spectra (lines) at $\theta=0°$ of these samples are shown for reference.

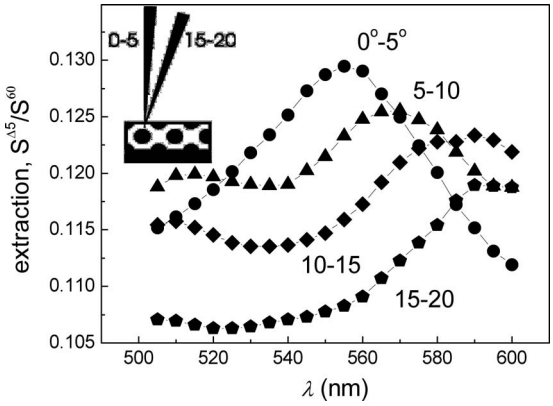

FIG. 9. Spectra of the 5°-wide emission flux fractions propagating along different directions. The schematic insert shows the difference between propagation directions of the 0–5 and 15–20 flux fractions.

for all studied LB-coated NCFs. In contrast, the $S_\lambda^5/S_\lambda^{60}$ fraction for the bare NCF increases monotonically across the same wavelength range.

By increasing the principal angle of the 5°-wide probe section, we observed that the extraction band follows the dispersion of the minimum of the far-field transmission spectra. This means that the extraction of radiation occurs in the direction of the transmission minimum, as it follows from the comparison of Figs. 9 and 5(a). At higher angles, the extraction band becomes less pronounced and distorted in response to the decreasing attenuation in the corresponding transmission minimum. It is worth noting that the resolution of other transmission minima is too poor to generate a corresponding flux maximum.

V. DISCUSSION

Observations of the emission spectrum and the emission diagram modifications are closely related to each other. They

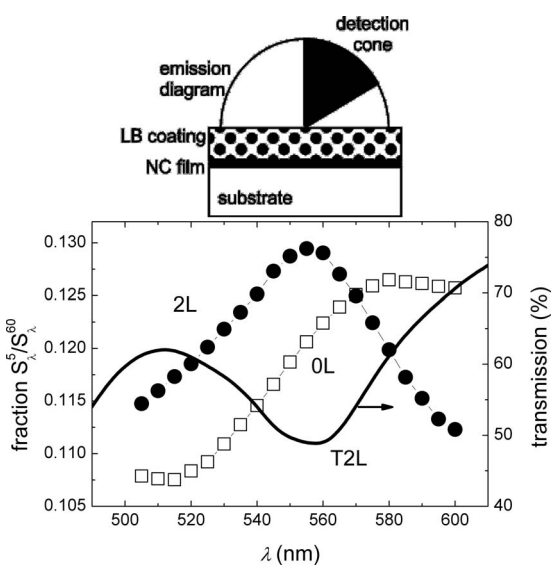

FIG. 8. Spectra of the emission flux fraction propagating along the film normal within a 5°-wide cone for bare (squares) and 2L-coated (circles) NCFs in comparison to the transmission spectrum of the 2L-coated NCF (line). The schematic explains the definition of 5°- and 60°-wide flux fractions.

can be associated either with grating-assisted outcoupling of the radiation from the NCF or with the effect of the PhC local field upon the NCF emitter. To choose the most probable mechanism we consider them in detail.

The first-order diffraction at periodically corrugated surface is widely used in light emitting devices for extraction of light trapped in the substrate due to total internal reflectance.[27,28] For example, the grating composed of a monolayer of silica spheres diffracts to the air the beam of 0.04 relative bandwidth from emission trapped in a glass substrate, which separates the grating from a source.[29]

The diffraction equation in this case relates the central wavelength of a diffraction peak λ_0 to the angle θ between the propagating beam and the substrate normal,

$$m\lambda_0 = \Lambda(\pm \sin\theta \pm \sin\alpha), \tag{1}$$

where α is the angle of diffraction with respect to the grating normal and Λ is the grating period. The interaction of modes guided in a substrate with a grating leads to a directional leakage of emission with λ_0.[30–32]

The grating diffraction in transmission was measured in LB films under the condition $\theta+\alpha=76°$ [Fig. 5(d)]. From the fit of $\lambda_0=\Lambda[\sin\theta+\sin(76°-\theta)]$ to the observed dispersion of this diffraction resonance [Fig. 3(c)] the grating period was extracted as $\Lambda=456$ nm. This is the half of the period $a=\sqrt{3}D$ of the trigonal lattice for the wave vector of incident light propagating along the ΓK direction in a Brillouin zone of a 2D hexagonal lattice, in which the distance between centers of spheres is 526 nm.

Substituting the grating periods $\Lambda_1=\sqrt{3}D/2$ and $\Lambda_2=D$ and the angle of incidence $\theta=90°$ into Eq. (1), we can obtain the angular dispersion of the light propagating along the substrate, which is diffracted by the 1L LB grating in the air [crosses in Fig. 3(b)]. Although there is a good correlation between the measured positions of the transmission minima at $\theta=0°$ and simulated diffraction, only branch IV in *p*-polarized light and the low-angle fraction of the branch III in both polarizations correlate with the surface diffraction dispersions.

However, the PhC-induced band in the relative PL spectra (empty squares in Fig. 10) follows the dispersion branch I of transmission minima observed in the *s*-polarized light,

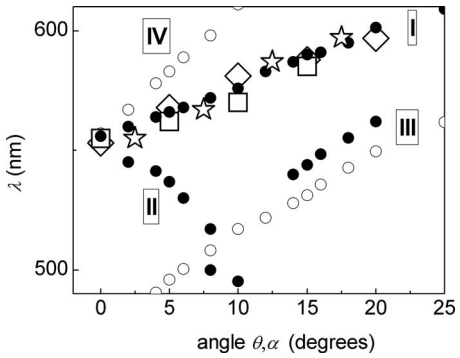

FIG. 10. Angular dispersion of transmission minima of a 2L LB coating in *s*- (solid circles) and *p*- (open circles) polarized lights. Empty squares (rhombs) represent the dispersion of the enhancement band in the forward (backward) relative PL spectra. Stars show the dispersion of peaks in radiation directionality spectra in Fig. 9.

which does not satisfy Eq. (1), a consideration of which shows that the enhanced PL band cannot be explained by the diffraction at the grating. This conclusion is also supported by comparison of the angle diagram of the intensity of the diffracted beam at $\lambda_0=550$ nm [crosses in Fig. 6(b)] and the emission intensity diagram at the same wavelength.

Another mechanism, the diffraction of the second order, assumes interaction of counterpropagating modes with the grating period and gives rise to the outcoupled beam with $\lambda_0=2n_{\mathrm{eff}}\Lambda/m$, where $m>1$, propagating within a very narrow radiation cone along the grating normal.[33,34] However, our observations do not satisfy this type of diffraction.

An alternative explanation of our observations takes into account the PBG structure of a 2D lattice of dielectric spheres. Such a PBG was calculated using the whispering gallery mode-coupling model.[21] This model explains reasonably well the observed far-field transmission spectra and their angular dependence. Moreover, this theory predicts considerable broadening of the minima bandwidth due to light leakage to the substrate.[35] The spectral position of the first bandgap in such PhC corresponds to the sphere diameter and the next gap takes place at a wavelength, which is lower by a factor of 1.21. The observed minima at 548 and 444 nm for 1L LB film are in good agreement with this model. Previously, we experimentally demonstrated that for LB colloidal crystals consisting of several sphere monolayers, a 2D model remains valid for the description of the PBG structure at wavelengths $\lambda\approx D$.[25]

Dips in transmission spectra of LB films appear due to light losses for the excitation of eigenmodes of the 2D PhC, which propagate in the LB film plane. At the PBG resonance, e.g., for $\theta\approx 0°$ at $\Lambda/\lambda\approx 1$,[6] the local field is enhanced due to large evanescent components of the electromagnetic field. It has been shown that the resonance enhances the intensity of a local field by two orders of magnitude if the monolayer of spheres is suspended in the air, whereas the attached substrate reduces the enhancement by factor of 10.[6,7,35]

The distribution of the local field at the surface of the opal-based PhC in the PBG wavelength range was modeled theoretically[36] and visualized by the near-field optical microscopy.[9] Since the near-field amplitude of evanescent waves decays rapidly away from a PhC surface on a scale of the PhC lattice constant, the NCF-based emitter should be in close proximity to a PhC surface. The strong local field promotes the spontaneous radiative recombination as compared to that in bare NCF. The apparent independence of the magnitude of the emission enhancement on the number of sphere layers in multiple-layer LB films correlates to the surface-related nature of the observed effect.

With this picture in mind, the PL spectrum transformation can be explained as follows. In the case of the bare NCF, the emission is coupled to the substrate and free space. In the presence of an LB coating, the formation of "hot spots" of the local field at PBG wavelengths along the PhC surface leads to a higher probability of the radiative recombination in the NCF at these spots. Since the relative PL spectrum demonstrates a peak at PBG wavelengths, we can tentatively assume that the acceleration of the radiative recombination in hot spots prevails over the recombination decrease at "cold" spots. The fact that the PBG in the far-field transmission corresponds to the peak in the emission intensity spectrum correlates the theoretical findings about the similarity of spectral features of 2D PhCs in the far and near fields.[36]

It should be emphasized that the PBG-related suppression of the emission intensity of PhC-embedded light sources is fundamentally different from the PBG emission control described in this paper. The dissimilarity relates to the different realizations of the coupling of a light source to a PhC. If the light source is embedded in a PhC with a directional PBG, there are no eigenmodes in the PBG spectral range to transport the emission along the PBG direction. Such emission suppression is conveniently observed in opal-based 3D PhCs impregnated with light emitters.[37–39] In contrast, if the light source is close to a PhC surface, it is not isolated from modes of free space, but subjected to the PhC local field, the magnitude of which is greatly enhanced in the PBG range. This increase in field magnitude is replicated in the increase in PL intensity.

The PBG origin of the PL spectrum modification leads to a spectrum directionality in agreement with the angular dispersion of the PBG minimum. The reason for the directionality is the dependence of the topology of the local field pattern on the wavelength. If the longitudinal wave vector of the emitted radiation at a given wavelength matches the lattice constant of a 2D PhC, the intensity of this radiation increases according to this particular hot spot pattern. The emission indicatrix (Fig. 9) in the studied case appears more sensitive to the PBG directionality compared to the directional spectrum changes (Fig. 5). Remarkably, the maximum in the directionality spectra follows that of the enhancement band of the relative PL spectra (stars in Fig. 10).

The strong argument in favor of the PBG mechanism of the emission enhancement is the correlation between the relative NCF PL spectra measured in the backward direction, for which the emission does not pass the LB crystal and the LB crystal transmission spectra (Fig. 11). The structure of the forward and backward relative PL spectra is similar, i.e., enhancement reveals itself in opposite directions simultaneously, although the influence of the PBG is weaker for the latter. The dispersion of the maxima in the backward relative PL spectra (rhombs in Fig. 10) follows exactly the same

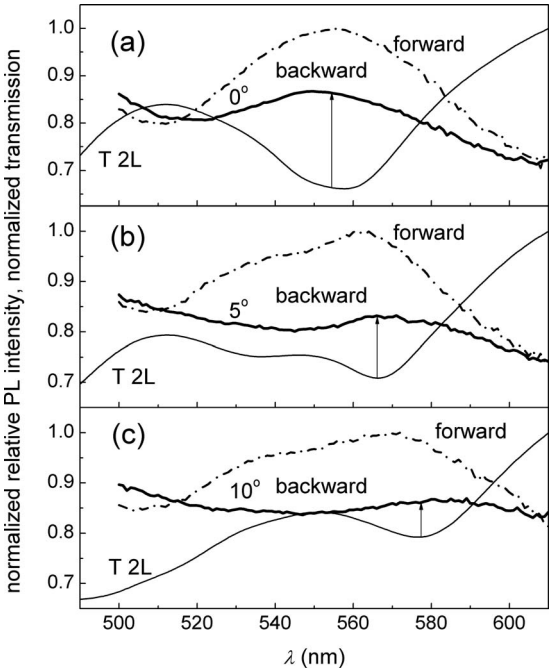

FIG. 11. Normalized angle-resolved transmission (thin solid line) and relative PL spectra at (a) 0°, (b) 5°, and (c) 10° of a 2L LB-coated NCF observed in the backward direction through the glass substrate (thick solid) and the forward direction through the LB crystal (dashed-dotted lines). Arrows indicate the centers of transmission minima.

dispersion as that in the forward spectra. These observations point to the fact that the NCF forms an interacting unit with the LB PhC.

VI. SUMMARY

Studies of the light emission from a source positioned at the surface of a colloidal PhC demonstrated a number of counterintuitive results. (1) The intensity of emission, which is radiated in the near-field zone of the colloidal PhC and passed through it along the direction of the PBG-related transmission minimum, is not suppressed in the spectral/directional range of this PBG, but, in contrast, it is enhanced relative to the emission outside the PBG. (2) The directionality of the enhanced emission flux does not satisfy the diffraction mechanism of the radiation outcoupling. (3) The radiation, which does not pass through the LB PhC, is the subject of similar spectrum modification as that which is detected behind the PhC. In our opinion, the observed phenomena relate to the (i) enhanced local field strength developed in the PBG spectral range at the PhC surface, which leads to the acceleration of the radiative relaxation of the affected light source, and (ii) the topology of the enhanced field pattern, which leads to selectivity of the emission coupling to PhC modes and, hence, directionality of radiation diagram.

The magnitude of the observed effects is small as compared to theoretical prediction; however, the studied architecture possesses the potential for the substantial improvement in the interaction between the light source and the PhC. Of particular interest would be the optimization of the coupling between the light source and the PhC using thinner NCFs, changing the RI of a substrate and increasing the RI contrast in the PhC.

ACKNOWLEDGMENTS

This work was supported in part by the Science Foundation Ireland, the EU NoE "Phoremost," (EU IST-511616) and the Russian RFBR (Grant No. 05-02-16975).

[1]E. M. Parcell, Phys. Rev. **69**, 681 (1946).
[2]V. P. Bykov, Sov. Phys. JETP **35**, 269 (1972); E. Yablonovitch, Phys. Rev. Lett. **58**, 2059 (1987); S. John, *ibid.* **58**, 2486 (1987).
[3]S. Noda, A. Chutinan, and M. Imada, Nature (London) **407**, 608 (2000).
[4]T. Yoshie, J. Vuckovic, A. Scherer, H. Chen, and D. Deppe, Appl. Phys. Lett. **79**, 4289 (2001).
[5]A. F. Koenderink, M. Kafesaki, C. M. Soukoulis, and V. Sandoghdar, J. Opt. Soc. Am. B **23**, 1196 (2006).
[6]M. Inoue, Phys. Rev. B **36**, 2852 (1987).
[7]Y. Kurokawa, H. Miyazaki, and Y. Jimba, Phys. Rev. B **69**, 155117 (2004).
[8]K. Ohtaka, H. Miyazaki, and T. Ueta, Mater. Sci. Eng., B **48**, 153 (1997).
[9]E. Fluck, N. F. van Hulst, W. L. Vos, and L. Kuipers, Phys. Rev. E **68**, 015601 (2003).
[10]H. Rigneault, F. Lemarchand, A. Sentenac, and H. Giovannini, Opt. Lett. **24**, 148 (1999).
[11]W. B. Joyce, R. Z. Bachrach, R. W. Dixon, and D. A. Sealer, J. Appl. Phys. **45**, 2229 (1974).
[12]P. Bermel, C. Luo, and J. D. Joannopoulos, Opt. Express **15**, 16986 (2007).
[13]M. Boroditsky, T. F. Krauss, R. Coccioli, R. Vrijen, R. Bhat, and E. Yablonovitch, Appl. Phys. Lett. **75**, 1036 (1999).
[14]S. G. Romanov, D. N. Chigrin, C. M. Sotomayor Torres, N. Gaponik, A. Eychmüller, and A. L. Rogach, Phys. Rev. E **69**, 046606 (2004).
[15]V. G. Solovyev, S. G. Romanov, C. M. Sotomayor Torres, M. Müller, R. Zentel, N. Gaponik, A. Eychmüller, and A. L. Rogach, J. Appl. Phys. **94**, 1205 (2003).
[16]P. Lodahl, A. F. van Driel, I. S. Nikolaev, A. Irman, K. Overgaag, D. Vanmaekelbergh, and W. L. Vos, Nature (London) **430**, 654 (2004).
[17]V. Shavel, N. Gaponik, and A. Eychmüller, Eur. J. Inorg. Chem. **2005**(18), 3613.
[18]M.-H. Lu and J. C. Strum, J. Appl. Phys. **91**, 595 (2002).
[19]Y. Xia, B. Gates, Y. Yin, and Y. Lu, Adv. Mater. (Weinheim, Ger.) **12**, 693 (2000).
[20]M. Bardosova, P. Hodge, L. Pach, M. E. Pemble, V. Smatko, R. H. Tredgold, and D. Whitehead, Thin Solid Films **437**, 276 (2003); S. Reculusa and S. Ravaine, Chem. Mater. **15**, 598 (2003).
[21]H. T. Miyazaki, H. Miyazaki, K. Ohtaka, and T. Sato, J. Appl. Phys. **87**, 7152 (2000).
[22]N. P. Gaponik, D. V. Talapin, A. L. Rogach, K. Hoppe, E. V. Shevchenko, A. Kornowski, A. Eychmüller, and H. Weller, J. Phys. Chem. B **106**, 7177 (2002).
[23]W. Stöber, A. Fink, and E. Bohn, J. Colloid Interface Sci. **26**, 62 (1968).
[24]M. Bardosova, P. Hodge, V. Smatko, R. H. Tredgold, and D. Whitehead, Acta Phys. Slov. **54**, 1 (2004).
[25]S. G. Romanov, M. Bardosova, M. Pemble, and C. M. Sotomayor Torres, Appl. Phys. Lett. **89**, 043105 (2006).
[26]S. G. Romanov, M. Bardosova, I. Povey, M. Pemble, and C. M. Sotomayor Torres, Appl. Phys. Lett. **90**, 133101 (2007).
[27]Zh. I. Alferov, V. M. Andreev, S. A. Gurevich, R. F. Kazariniv, V. R. Larionov, M. N. Mizerov, and E. L. Portnoi, IEEE J. Quantum Electron. **11**, 449 (1975).
[28]G. A. Turnbull, P. Andrew, M. J. Jory, W. L. Barnes, and I. D. W. Samuel, Phys. Rev. B **64**, 125122 (2001).
[29]T. Yamasaki, K. Sumioka, and T. Tsutsui, Appl. Phys. Lett. **76**, 1243 (2000).
[30]M. L. Dakss, L. Khun, P. F. Heidrich, and B. A. Scott, Appl. Phys. Lett. **16**, 523 (1970).
[31]B. J. Matterson, J. M. Lupton, A. F. Safonov, M. G. Salt, Wi. L. Barnes, and I. D. W. Samuel, Adv. Mater. (Weinheim, Ger.) **13**, 123 (2001).
[32]J. M. Ziebarth, A. K. Saafir, S. Fan, and M. D. McGehee, Adv. Funct. Mater. **14**, 451 (2004).
[33]W. Streifer, D. R. Scifres, and R. D. Burnham, IEEE J. Quantum Electron. **13**, 134 (1977).

[34]M. Kanskar, P. Paddon, V. Pacradouni, R. Morin, A. Busch, J. F. Young, S. R. Johnson, J. MacKenzie, and T. Tiedje, Appl. Phys. Lett. **70**, 1438 (1997).
[35]Y. Kurokawa, H. Miyazaki, and Y. Jimba, Phys. Rev. B **65**, 201102 (2002).
[36]H. Miyazaki and K. Ohtaka, Phys. Rev. B **58**, 6920 (1998).
[37]S. G. Romanov, A. V. Fokin, V. I. Alperovich, N. P. Johnson, and R. M. De La Rue, Phys. Status Solidi A **164**, 169 (1997).
[38]V. N. Bogomolov, S. V. Gaponenko, I. N. Germanenko, A. M. Kapitonov, E. P. Petrov, N. V. Gaponenko, A. V. Prokofiev, A. N. Ponyavina, N. I. Silvanovich, and S. M. Samoilovich, Phys. Rev. E **55**, 7619 (1997).
[39]S. G. Romanov, D. N. Chigrin, V. G. Solovyev, T. Maka, N. Gaponik, A. Eychmüller, A. L. Rogach, and C. M. Sotomayor Torres, Phys. Status Solidi A **197**, 662 (2003).